Load Transient Response Analysis of Constant On-Time DC–DC Converters Using a State-Variables Approach

Federico Bizzarri, *Senior Member, IEEE*, Paolo Nora, and Angelo Brambilla, *Member, IEEE*

***Abstract*—In the design of constant-on-time buck converters, prediction of the onset of subharmonics, at steady-state working conditions, and prediction of the saturation of the controller, i.e., the occurrence of at least one switching cycle at minimum OFF-time, after a dynamic step variation of the load are relevant aspects. By starting from the design parameters of a constant-on-time buck converter and grounding on a state-variables approach, we consider these aspects and develop a reliable and efficient approach to determine both limits. The proposed approach, despite having rigorous mathematical basis, is sufficiently simple. Thus it can be easily applied to predict results in designing constant-on time buck converters. The accuracy and effectiveness of the proposed approach is tested versus experimental results. This article is accompanied by a MATLAB live script that allows the reader to reproduce the proposed results and create new case studies.**

***Index Terms*—Constant ON-time buck converter (COT), equivalent series resistance (ERS), load transient, pulse bursting.**

I. Introduction

CONSTANT ON-time dc–dc converters have gained much popularity for point-of-load (POL) regulation [1], [2]. Their potentially excellent dynamic response makes constant ON-time (COT) POL regulators an attractive choice for powering demanding, high-speed digital loads such as FPGAs, ASICs, and CPUs. Existing technical literature often deals with small-signal analysis and modeling of COTs or emphasizes the achievable dynamic response due to the ease of control saturation [3]. However it often fails to provide an analytical method to predict large-signal system dynamics, and especially the output voltage deviation under a given large-signal load transient stimulus [4]–[7]. This article attempts to fill this gap, by resorting to a state-variables approach, providing a two-fold contribution.

1) We derive a sufficient condition to avoid the onset of the pulse-bursting phenomenon or subharmonics [8]–[11]. This condition is valid not only when the COT works in steady state but also during transient evolutions. Literature already reports condition on COT parameters that avoids these drawbacks [10], [11]. The condition described in this article is more articulated and considers several design parameters of the COT converter, for example the input power supply voltage, the value of the inductor and output capacitor, the equivalent series resistance (ESR) of the output capacitor.
2) We derive a sufficient condition to check if the COT converter saturates the controller when the load resistance is instantaneously reduced. This corresponds to a duration of the OFF-phase that reaches its minimum allowed value. Instantaneous reduction models the worst-case condition on load increase. This is a very important data-point from practical design perspective, because it tells the designer that from that point on the dynamics of the inductor current and in particular its rate-of-rise starts to be determined only by the ratio of Δt_{ON} to $\Delta t_{\mathrm{OFF}}^{\mathrm{min}}$, the input and output voltages, and the inductor value itself [12].

   The condition on saturation of the controller can be exploited with two different perspectives. To check if saturation occurs viz., the COT converter is able to work at its maximum speed performance when the load undergoes its maximum designed power step. To check if saturation does not occur, if one is interested in guaranteeing that the regulation of the output voltage is not lost.

We focus on a COT dc–dc converter architecture (a typical one is shown in Fig. 1) that, despite being simplified, sounds to be still very relevant from the practical viewpoint. Simplification, which is necessary to achieve a state-space model of the COT converter allowing simple but significant considerations on its dynamical behavior, is related with the management of the *equivalent inductor current ripple waveform* that, superimposed to the feedback signal, plays a significant role in typical COT control methods. Here it is assumed to act on the equivalent inductor-current ripple waveform only by means of the R_e ESR resistance (see Fig. 1) and a discussion in support of this choice is provided in Section II-A.

Manuscript received May 11, 2019; revised August 1, 2019; accepted September 3, 2019. Date of publication September 15, 2019; date of current version February 11, 2020. Recommended for publication by Associate Editor M. Chen. *(Corresponding author: Federico Bizzarri.)*

F. Bizzarri is with the Politecnico di Milano, 20133 Milano, Italy, and also with the Advanced Research Center on Electronic Systems for Information and Communication Technologies E. De Castro (ARCES), University of Bologna, 41026 Bologna, Italy (e-mail: federico.bizzarri@polimi.it).

P. Nora is with the Microchip Technology, 20025 Legnano, Italy (e-mail: paolo.nora@microchip.com).

A. Brambilla is with the Politecnico di Milano, 20133 Milano, Italy (e-mail: angelo.brambilla@polimi.it).

This article has supplementary downloadable material available at http://ieeexplore.ieee.org, provided by the author.

Color versions of one or more of the figures in this article are available online at http://ieeexplore.ieee.org.

Digital Object Identifier 10.1109/TPEL.2019.2941756

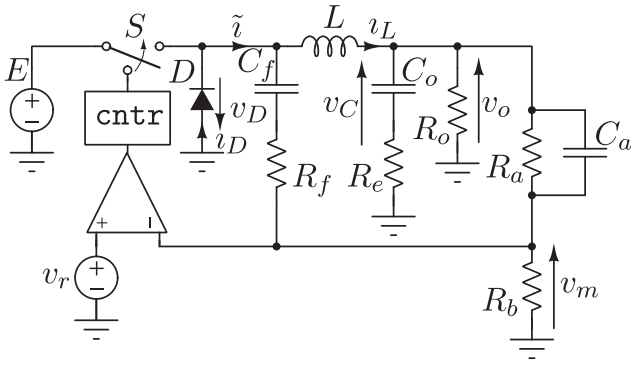

Fig. 1. Schematic of COT converter. The C_a and C_f capacitors together with the R_f resistance will be neglected in our theoretical study. They are typically used to provide the capacitor C_o with a "virtual" ESR higher than the R_e built-in one.

The article is organized as follows. In Section II, after a detailed discussion concerning the approach adopted here to control the equivalent inductor-current ripple waveform of the COT converter, the state-space model of the circuit is derived taking into account the switching rules set by its controller block. Moreover, the typical structure of its steady state trajectories is discussed. Sections III and IV are devoted to derive and discuss the two above-mentioned conditions. In Section V simulation results and experimental measurements are presented to validate our approach. Finally, some conclusions are drawn.

II. Modeling the COT Converter Dynamics

The schematic of the COT converter considered in this article is shown in Fig. 1.

A. On the Equivalent Inductor-Current Ripple Waveform

In this section, the mechanisms to provide equivalent inductor-current ripple are discussed. This is relevant since, for instance, many POL dc–dc converters often use standard multilayer ceramic capacitors (MLCCs) in the output filter. Due to the low ESR of MLCCs, the output voltage waveform by itself may not have enough inductor current equivalent ripple, or the inductor current equivalent ripple might be too small in comparison to its capacitive counterpart. This in turn generates instability phenomena [10], [11]. To overcome this issue, an artificial ramp, which is in phase with the inductor current ripple, is often added to the feedback signal.

Several methods of external and internal ripple injection were proposed [13], [14]. One example of ripple injection network in a commercial COT converter [15] is shown in Fig. 1. The C_f and C_a capacitors and the R_f resistor are used to provide additional ripple to the feedback waveform, such that the capacitor C_o appears to have a "virtual" ESR R_e higher than the physical one.

Other methods include the increase of the series resistance of the output capacitor, either by using available capacitors with higher ESR, or by physically adding a series resistor [16]. This method was often considered incompatible with the power supply requirements of modern high-speed electronics. However, output impedance analysis [17] indicates that the low and poorly controlled ESR of standard MLCCs may generate an output impedance profile which is prone to the rogue wave phenomenon [18]. This should be avoided for risk mitigation purposes, especially when it comes to powering demanding high-speed digital devices whose load current pattern is hardly predictable. Also because of this reason, MLCC and high-performance digital device vendors have increasingly been focusing on the use of better controlled-ESR, low-ESR ceramic capacitors [19], [20]. In such cases, artificial ripple injection may not even be necessary because the output capacitors already have enough ESR. Furthermore, the increased switching-frequency ripple due to higher series resistance of the output capacitor can be balanced against smaller output voltage deviations in load transient. Especially for high-speed digital loads, any deviation of the output voltage must be bounded within specified limits, regardless if it is contributed by a steady state repetitive perturbation—such as switching-frequency ripple—or by a load transient response [21].

In this article, the artificial ripple injection components R_f, C_f, and C_a will be neglected, thus obtaining $\imath_L \equiv \tilde{\imath}$ and reducing the state variables of the circuit to $\imath_L$ and v_C only. The ripple is only created by means of a series resistance R_e rather than by a ripple injection network. In light of the considerations mentioned above, this simplified approach is still very relevant from the practical viewpoint.

Furthermore, the considered load is purely resistive (see the R_o resistor in Fig. 1). This choice is justified since we are mainly interested in strongly dynamic, fast modern digital loads. Power dissipation of CMOS logic, working in its currently narrow operating range, is well modeled by a purely resistive load equivalent [22]. The power delivered by the COT converter is proportional to the square of the (almost constant) applied voltage divided by the load equivalent resistance.

B. Controller and the Switching Rules

This section is devoted to the COT converter control algorithm implemented in the `cntr` block. It can be summarized as follows.

- `Step 1:` Any time $v_r - v_m$ gets positive, the output of the comparator becomes positive, the controller catches the positive edge of this signal and the S switch is closed for the Δt_{ON} *fixed* time interval (ON-phase).
- `Step 2:` At the end of the ON-phase, S is opened and is kept open for the $\Delta t_{\text{OFF}}^{\min}$ *fixed* time interval (minimum OFF-phase).
- `Step 3:` At the end of the $\Delta t_{\text{ON}} + \Delta t_{\text{OFF}}^{\min}$ time interval, the controller checks the output of the comparator. If $v_r - v_m < 0$, the S switch remains open (OFF-phase) until the condition at `Step 1` becomes true. Otherwise, if $v_r - v_m > 0$, i.e., the output of the comparator is still positive, the S switch is closed again and a new ON-phase starts immediately. The overall duration of the OFF-phase is $\Delta t_{\text{OFF}} \geq \Delta t_{\text{OFF}}^{\min}$.

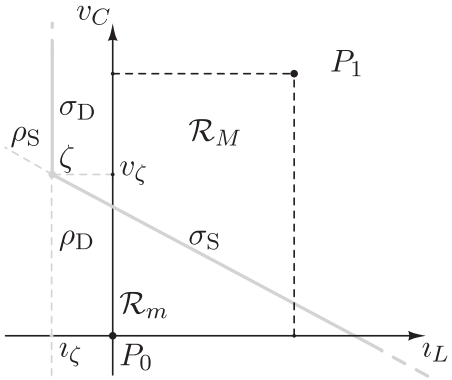

Fig. 2. Basic geometrical elements on the $(\imath_L, v_C)$ state plane.

$\Delta t_{\rm OFF}^{\rm min}$ is necessary in practical designs for various reasons, which include, for example, reliable implementation of anticross conduction control of the power switches, the recharge of the bootstrap capacitor in N-channel high-side topologies, or the acquisition of the current signal during the OFF-phase for circuit protection purposes.

The role of the D diode in Fig. 1 is to avoid a negative $\tilde{\imath}$ current. Actually, in modern architectures, such as synchronous buck converters, to enhance converter efficiency the diode is replaced by a low-side MOSFET which is operated as a synchronous rectifier. Consequently, "diode" D – that actually works as a controlled switch in perfect "diode emulation" is modeled as a piecewise-linear ideal component with $\imath_D = 0$ for $v_D \leq 0$ and $v_D = 0$ for $\imath_D \geq 0$. Furthermore, acting on the limitation of the reverse current of this device, it is possible to have $\tilde{\imath} \geq \imath_\zeta$ with $\imath_\zeta \leq 0$. Without loss of generality, boundary $\imath_\zeta$ can be set to very negative values if reverse current limit is not implemented by the low-side synchronous rectifier switch.

A resistor R_p (not shown in Fig. 1) is used to model both the ON-state resistance of the S high-side switch and the D low-side switch.

In the $(\imath_L, v_C)$ state plane (shown in Fig. 2) the $v_r - v_m = 0$ switching condition induced by the `cntr` block leads to the straight line

$$\rho_S(\imath_L, v_C) : v_r - \underbrace{\frac{R_b R_o(\imath_L R_e + v_C)}{R_{ab}R_e + (R_{ab}+R_e)R_o}}_{v_m} = 0 \qquad (1)$$

where $R_{ab} = R_a + R_b$. The normal vector to ρ_S is

$$\eta = (1, R_e)^{\rm T} \qquad (2)$$

and in the following it will play a significant role in determining a sufficient condition to avoid steady state solutions made up of more than a single ON-phase and OFF-phase (subharmonics). The effect of the D low-side switch defines $\rho_D(\imath_L, v_C)$: $\imath_L - \imath_\zeta = 0$.

C. State-Space Model

The state equations governing the dynamics of the v_C voltage and the $\imath_L$ current (for $\imath_L > \imath_\zeta$) are

$$\begin{aligned} \dot{v}_C &= \frac{R_{ab}R_o\imath_L - (R_{ab}+R_o)v_C}{C_o(R_{ab}R_e + (R_{ab}+R_e)R_o)} \\ \dot{\imath}_L &= -\frac{R_{ab}R_o v_C}{L_o(R_{ab}R_e + (R_{ab}+R_e)R_o)} \\ &\quad -\frac{(R_{ab}R_eR_o + (R_{ab}R_e + (R_{ab}+R_e)R_o)R_p)\imath_L}{L_o(R_{ab}R_e + (R_{ab}+R_e)R_o)} + \xi\frac{E}{L_o} \end{aligned} \qquad (3)$$

where $\xi = 1$ in the ON-phase and $\xi = 0$ in the OFF one. Equation (3) describes a *switched affine* dynamical system that admits the two

$$P_\xi = \left(\frac{ER_{ab}R_o\xi}{R_{ab}R_o + (R_{ab}+R_o)R_p}, \frac{E(R_{ab}+R_o)\xi}{R_{ab}R_o + (R_{ab}+R_o)R_p}\right) \qquad (4)$$

different equilibria for $\xi \in \{0, 1\}$ (see Fig. 2). P_0 and P_1 represent, respectively, the equilibrium points reached if the OFF and the ON phases would last forever. Hence the generic orbit of (3) is attracted by either P_1 or P_0, during the ON-phase or the OFF-phase, respectively and it visits the $\mathcal{R}_m \cup \mathcal{R}_M$ region (see Fig. 2). The $\mathcal{R}_m$ (resp. $\mathcal{R}_M$) subregion of the state-space is made up of those points lying both at the right of the ρ_D line and below (resp. above) the ρ_S line. $\mathcal{R}_m$ and $\mathcal{R}_M$ are separated by the half-line $\sigma_S \subset \rho_S$ that originates in ζ.

D. On the Structure of the Steady State Solutions

This section is devoted to the geometry of the steady state solution of a "well behaving" COT converter. The existence of subharmonic regimes is discussed too and the continuous current mode (CCM) and discontinuous current mode (DCM) operation conditions are introduced.

According to the very definition of the `cntr` block, a generic orbit of the COT converter is made up of a sequence of $\Gamma_{\rm ON}^{(k)} - \Gamma_{\rm OFF}^{(k)}$ segments being $k = 1, \ldots, K$ with $K \geq 1$. At (periodic) steady state, the last point of $\Gamma_{\rm OFF}^{(K)}$ equals the first point of $\Gamma_{\rm ON}^{(1)}$. In Fig. 3 two examples of closed orbits can be observed. Each one of these orbits is made up of two segments. The orbit passing through the α_k points (for $k = 1, \ldots, 4$) includes the segments $\Gamma_{\rm ON}^{(1)} - \Gamma_{\rm OFF}^{(1)}$ and $\Gamma_{\rm ON}^{(2)} - \Gamma_{\rm OFF}^{(2)}$. The former goes from α_1 to α_3 through α_2, whereas the latter goes from α_3 to α_1 through α_4. In principle the K OFF-phases are characterized by different durations and at least one of the $\Gamma_{\rm ON}^{(k)} - \Gamma_{\rm OFF}^{(k)}$ segments is originated on σ_S (see Fig. 3). In the following, a limit cycle made up of only one $\Gamma_{\rm ON}^{(1)} - \Gamma_{\rm OFF}^{(1)}$ segment is referred to as *single-segment limit cycle*.

If the limit cycle is born from a generic point on $\sigma_S \backslash \{\zeta\}$ and in the OFF-phase the orbit does not hits σ_D, then the system is operating in CCM, without engaging negative inductor current limitation.

The $\sigma_{\rm ON}$ half-line in Fig. 3 is the locus of points that are reached in $\Delta t_{\rm ON}$ (at the end of the ON-phase) by orbits originated on $\sigma_{\rm S}$. Once $\sigma_{\rm ON}$ is hit, the orbits continue their evolution and

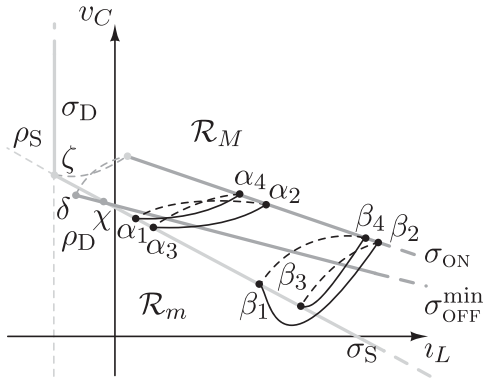

Fig. 3. Half-line $\sigma_{\rm ON}$ is the locus of points reached at the end of the fixed-duration ON-phase by orbits originated on σ_S. The half-line $\sigma_{\rm OFF}^{\rm min}$ is the locus of points reached in $\Delta t_{\rm OFF}^{\rm min}$ by orbits originated on $\sigma_{\rm ON}$. The orbit from $\sigma_{\rm ON}$ reaching $\sigma_{\rm OFF}^{\rm min}$ in χ corresponds to the OFF-phase with the minimum allowed duration. The points β_k ($k = 1, \ldots, 4$) identify a $\mathcal{C}_{\rm II}$ two-segment limit cycle.

in $\Delta t_{\rm OFF}^{\rm min}$ (i.e., during the mandatory portion of the OFF-phase) they come to the $\sigma_{\rm OFF}^{\rm min}$ half-line. Both $\sigma_{\rm OFF}^{\rm min}$ and $\sigma_{\rm ON}$ can be computed analytically. A single-segment limit cycle is *minimum* if $\Delta t_{\rm OFF} = \Delta t_{\rm OFF}^{\rm min}$. In this case $\chi = \sigma_{\rm OFF}^{\rm min} \cap \sigma_S$, corresponds to the origin of the $\Gamma_{\rm ON}^{(1)} - \Gamma_{\rm OFF}^{(1)}$ segment.

Two-segment steady state solutions can be of two different types. A first class, say $\mathcal{C}_{\rm I}$, is made up of limit cycles whose $\Gamma_{\rm ON}^{(1)} - \Gamma_{\rm OFF}^{(1)}$ segment originates on σ_S but its last point lies in $\mathcal{R}_m$. In this case, according to `Step 3` of the `cntr` block, the OFF-phase lasts $\Delta t_{\rm OFF}^{\rm min}$, a second ON-phase is originated in $\mathcal{R}_m$, the trajectory reaches $\mathcal{R}_M$ and the last point of the $\Gamma_{\rm ON}^{(2)} - \Gamma_{\rm OFF}^{(2)}$ segment closes the limit cycle on σ_S. The duration of this last segment is generically greater than $\Delta t_{\rm OFF}^{\rm min}$. The $\mathcal{C}_{\rm II}$ second class of two-segment steady state solutions exhibits a first segment that originates on σ_S and reaches again σ_S (from $\mathcal{R}_M$) in a point not corresponding to its first one. As a consequence a further pair of ON-phase and OFF-phase is started that ends on the initial point of the limit cycle (see the trajectory passing through the β_k points in Fig. 3 for $k = 1, \ldots, 4$). The orbits in $\mathcal{C}_{\rm I}$ and $\mathcal{C}_{\rm II}$ lead to typically undesirable subharmonic regimes [8], [10]. We thus consider only $\Gamma_{\rm ON}^{(1)} - \Gamma_{\rm OFF}^{(1)}$ limit cycles, and define operative conditions to guarantee the existence of such a dynamical behavior.[1]

If in the ON-phase the limit cycle is born from ζ and in the OFF-phase the orbit hits σ_D, the limitation of the reverse current of the low-side MOSFET is reached. If the limitation value is set to 0, this condition is equivalent to the onset of DCM. In this case the evolution of the system trajectory in the state space becomes more complex since it also depends on the particular protection strategy against excessive negative current. In many practical

[1]The structure of the described limit cycles can be generalized thus considering more generic cases for $K > 2$. Nevertheless it is not particularly meaningful since typically a COT converter is assumed to *properly* work at steady state if it exhibits a nonminimum single-segment limit cycle. Multisegments limit cycles are highly undesirable since they will cause an increase in the ripple of the inductor current and of the output voltage, with significant efficiency degradation.

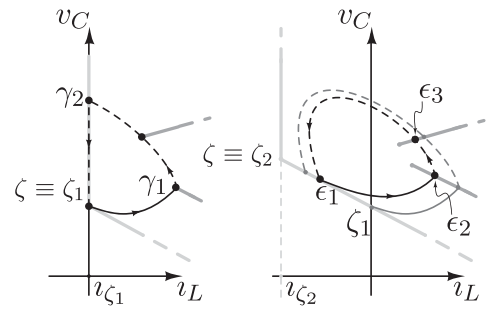

Fig. 4. In the left panel, a DCM steady-state trajectory hitting σ_D and sliding on it obtained by setting $\imath_{\zeta_1} = 0$. In the right panel, a CCM steady state trajectory obtained by setting $\imath_{\zeta_2} < \imath_{\zeta_1}$.

cases, the low-side switch will be turned OFF, thus causing the inductor current to decay (down to 0 or just for some amount of time) by discharging its energy on the input supply voltage E through the body-diode of the high-side MOSFET. This also implies a topological change of the circuit. Since the dynamics is very much dependent on the particular circuit implementation and it is only activated in abnormal operating conditions, it will not be considered in the following discussion.

The structure of the system trajectory are certainly less involved in the classic DCM case, where the low-side MOSFET works as a simple diode, since in this case it can be reasonably assumed that once the trajectory hits σ_D it immediately slides on it till ζ is reached. This situation is reported in the left panel of Fig. 4 where the DCM steady state trajectory passing through ζ_1 and the γ_k points (for $k \in \{1, 2\}$) is shown. In the following, when referring to DCM, only the $\imath_\zeta = 0$ case will be considered. When the trajectory slides on σ_D, (3) reduces to

$$\dot{v}_C = -\frac{(R_{ab} + R_o)v_C}{C_o(R_{ab}R_e + (R_{ab} + R_e)R_o)} i_L = 0.$$

The boundary between CCM and DCM, often referred to as *critical conduction mode*, is observed in the limit case when the limit cycle is born from ζ and ends in ζ but in the OFF-phase the orbit does not visit σ_D. It is possible to identify the limit value $R_o^{\rm CrCM}$ such that for $R_o < R_o^{\rm CrCM}$ CCM steady-state behavior is guaranteed. To identify $R_o^{\rm CrCM}$, as it has been done in the MATLAB live script accompanying this article, it is possible to setup a nonlinear optimization problem in two variables, i.e., R_o and $\Delta t_{\rm OFF}$. The $\Gamma_{\rm ON}^{(1)} - \Gamma_{\rm OFF}^{(1)}$ segment originated in ζ is computed for an initial guess of both R_o and $\Delta t_{\rm OFF}$. The distance between the last point of $\Gamma_{\rm ON}^{(1)} - \Gamma_{\rm OFF}^{(1)}$ and ζ is then computed and the value of R_o and $\Delta t_{\rm OFF}$ is properly updated by the `fsolve` MATLAB function. In other words, the optimization problem aims at minimizing the distance between the last point of $\Gamma_{\rm ON}^{(1)} - \Gamma_{\rm OFF}^{(1)}$ and ζ as a function of R_o and $\Delta t_{\rm OFF}$.

If we assume to be able to set $\imath_\zeta \ll 0$ then the system can be assumed to always work in CCM even in the case of large negative inductor currents. It is exemplified in the right panel of Fig. 4 where $\imath_{\zeta_2} < \imath_{\zeta_1} = 0$ and the CCM steady-state trajectory passing through the ϵ_k points (for $k = 1, \ldots, 3$) is represented.

This is often referred to as forced-pulsewidth modulation (PWM) (FPWM) mode of operation, which is particularly interesting in applications requiring a high-performance load-transient response and/or a more predictable switching frequency as load varies.

III. More on the COT Dynamics: Transient and Steady State

A. Engaging Minimum OFF-Phases

In this section, a limit value for R_o is derived such that every regular OFF-phase, i.e., originated on $\sigma_{\rm ON}$, is guaranteed to be not minimum ($\Delta t_{\rm OFF} > \Delta t_{\rm OFF}^{\rm min}$).

A COT converter ensuring that at *steady state* $\Delta t_{\rm OFF} > \Delta t_{\rm OFF}^{\rm min}$ can be designed by resorting to well known rules available in the literature, however existing design techniques do not provide guidelines to predict the onset of *transient* minimum OFF-phases as the applied load current step increases in magnitude. This behavior marks the onset of control saturation since the controller begins to be no longer able to act on $\Delta t_{\rm OFF}$. This is a very important data-point from practical design perspective, since it tells the designer that the dynamics of the inductor current, and in particular its rate-of-rise, starts to be determined only by the ratio of $\Delta t_{\rm ON}$ to $\Delta t_{\rm OFF}^{\rm min}$, the input and output voltages, and the inductor value itself. For example the onset of this condition tells the designer that the COT converter correctly saturates for a given step variation of the load equivalent resistance, i.e., the COT converter "reacts by jumping" at its maximum designed speed. On the other hand the designer can use the same information in a different way, determining what is the maximum load power step variation above which the COT controller saturates loosing load voltage control.

As far as we know, it was not possible to determine the step variation of R_o ensuring that every OFF-phase orbit, which is originated by definition on $\sigma_{\rm ON}$ returns on σ_S in $\Delta t_{\rm OFF} > \Delta t_{\rm OFF}^{\rm min}$. In CCM, this can be safely done by imposing that the δ origin of $\sigma_{\rm OFF}^{\rm min}$, i.e., the point that the trajectory originated in ζ (see Fig. 3) reaches after $\Delta t_{\rm ON} + \Delta t_{\rm OFF}^{\rm min}$, lies in $\mathcal{R}_M$. The limit condition $\chi \equiv \delta \in \sigma_S$, which results in $R_o \equiv R_o^{\delta\chi}$ can be, in principle, analytically determined. In particular, it is possible to find the $[\imath_L(\Delta t_{\rm ON}), v_C(\Delta t_{\rm ON})]$ solution of (3) at $t = \Delta t_{\rm ON}$, having assumed $\xi = 1$ and the $(\imath_\zeta, v_\zeta)$ initial condition at $t = 0$. Equation (3) is solved once more to derive $[\imath_L(\Delta t_{\rm OFF}^{\rm min}), v_C(\Delta t_{\rm OFF}^{\rm min})]$, by choosing $\xi = 0$ and the $[\imath_L(\Delta t_{\rm ON}), v_C(\Delta t_{\rm ON})]$ initial condition at $t = 0$.[2] Finally, the constraint $\rho_S(\imath_L(\Delta t_{\rm OFF}^{\rm min}), v_C(\Delta t_{\rm OFF}^{\rm min})) = 0$ is imposed [see (1)]. This relation depends on the COT converter parameters. It is possible to identify the value of one of those (having fixed the others) so that the relation itself is satisfied. If this is done w.r.t. R_o, then $R_o^{\delta\chi}$ can be achieved.[3]

[2]Note that (3) models an autonomous dynamical system and consequently we can choose $t = 0$ also to evaluate the evolution in the OFF-phase.

[3]As far as CrCM and DCM are concerned, the calculation of the boundary value of R_o is of no practical interest and it will be neglected. As a matter of fact, if CrCM or DCM occur within a $\Delta t_{\rm OFF}^{\rm min}$ during a load step increase, this implies that the inductor current is reset to zero before or exactly at $\Delta t_{\rm OFF}^{\rm min}$. This can only occur under very unsuitable choices of design parameters which are not found in practical examples.

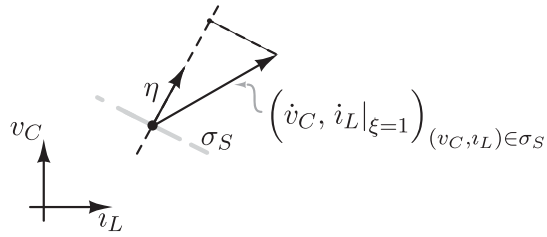

Fig. 5. Geometrical representation of the constraint provided by (5). A trajectory originated at a generic point on σ_S at the beginning of the ON-phase [$\xi = 1$ in (3)] is governed by the vector field $(\dot v_C, i_L|_{\xi=1})_{(v_C,\imath_L)\in\sigma_S}$ charaterized by a nonnull component orthogonal to σ_S.

B. Avoiding Pulse-Bursting: The Bouncing Condition

In this section, a sufficient condition to ensure that the COT converter operates without pulse bursting is derived [8]. To avoid the existence of two-segment (or more) limit cycles, it is important to realize that they can exist only if the orbit originated in σ_S is allowed to visit $\mathcal{R}_m$. This is trivial for what concerns $\mathcal{C}_{\rm I}$ whereas for $\mathcal{C}_{\rm II}$ it is necessary to recall that, for a fixed value of ξ, (3) models an autonomous dynamical system and consequently its orbits can not intersect. With this in mind, by observing the sketches in Fig. 3, we should conclude that the closed trajectory originated in α_1 is not allowed since the dashed orbits, that would be solutions of (3) with $\xi = 0$, do intersect. On the contrary, the closed trajectory originated in β_1 does not exhibit any intersections neither of the dashed orbits nor of the solid ones. This is possible since the $\beta_1 - \beta_2$ segment visits $\mathcal{R}_m$. Therefore we introduce the condition

$$\eta^{\rm T} \cdot \left(\dot v_C,\, i_L|_{\xi=1}\right)_{(v_C,\imath_L)\in\sigma_S} > 0 \tag{5}$$

that forces the vector-field in (3), computed for any point on σ_S at the beginning of the ON-phase, to "push" the state of the system in $\mathcal{R}_M$ [η has been defined in (2)]. A geometrical representation of this constraint, which is a standard in the realm of hybrid dynamical systems [23], is shown in Fig. 5. In other words, if a generic orbit in $\mathcal{R}_M$ is seen as the trajectory of a particle moving in a planar subspace, σ_S is a reflective boundary that allows neither penetration (towards $\mathcal{R}_m$) nor sliding on it. In terms of the v_o output voltage of the COT converter, if (5) holds we have $v_o \geq \frac{R_{ab} v_r}{R_b}$ during the ON-phase. If (5) is satisfied for any point of σ_S when generically applied to transient ON-phase orbits, in particular it is valid at steady state. Consequently it allows to avoid $\mathcal{C}_{\rm II}$ solutions.

(5) leads to

$$\frac{\bar\imath_L R_o \Xi - L_o(R_{ab} + R_o) v_r + C_o R_e R_o (E R_b - R_{ab} v_r)}{C_o L_o R_b R_o} > 0 \tag{6}$$

where $\Xi = R_b(L_o - C_o R_e R_p)$ and $\bar\imath_L = \imath_L|_{(v_C,\imath_L)\in\sigma_S}$. This is one of the two relevant results presented in this article.

A more restrictive condition not depending on $\bar\imath_L$ is obtained assuming $\Xi \geq 0$.[4] Under this assumption, being $\imath_\zeta \leq 0 \leq \bar\imath_L$,

[4]To assume $\Xi \geq 0$ is realistic since ideally one would like to have $R_p \to 0$. Obviously this is not feasible but nevertheless it is easy to have $L_o > C_o R_e R_p$.

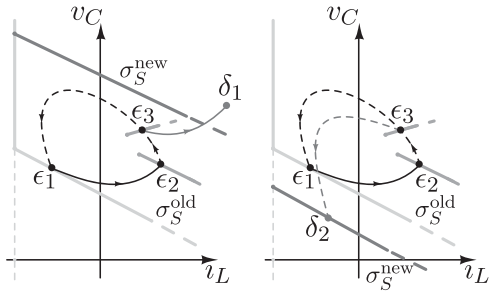

Fig. 6. In both panels it is assumed that the load-transient starts when the steady state trajectory is in $\epsilon_3 \in \sigma_{\text{OFF}}^{\min}(R_o^{\text{old}})$. In the left panel $R_o^{\text{new}} < R_o^{\text{old}}$ and σ_S^{new} moves above σ_S^{old} whereas in the right panel $R_o^{\text{new}} > R_o^{\text{old}}$ and σ_S^{new} moves below σ_S^{old}.

(6) is tightened and reduces to

$$R_o > \frac{L_o R_{ab} v_r}{\imath_\zeta \Xi + C_o E R_b R_e - (L_o + C_o R_{ab} R_e) v_r} \equiv R_o^{\lim}. \quad (7)$$

Condition (7) is valid in both CCM and DCM since it is related to the ON-phase; in DCM, the condition becomes exact since the steady-state trajectory visits σ_S in $\bar{\imath}_L = \imath_\zeta = 0$ only.

In the Appendix B, we show how the popular $2C_oR_e > \Delta t_{\text{ON}}$ stability condition can be derived from (6) [6], [10].

IV. Predicting Control Saturation in Load Transients

By varying the value of the R_o output resistance, the σ_S manifold is vertically shifted in the $(\imath_L, v_C)$ plane keeping its normal vector η unchanged [see (2)]. In particular, if $R_o \to 0$, the intersection of σ_S with the v_C axis goes to infinity, whereas if $R_o \to \infty$, it goes to $v_r\,{}^{(R_{ab}+R_e)}/_{R_b}$.

The load-transient analysis is carried out by considering an instantaneous step variation of the output resistance R_o from its current value, say R_o^{old}, to the new R_o^{new} value. This is critical in predicting the saturation of the controller of the COT converter.

By defining $\sigma_S^{\text{old}} \equiv \sigma_S(R_o^{\text{old}})$ and $\sigma_S^{\text{new}} \equiv \sigma_S(R_o^{\text{new}})$, it is possible that the latter moves over so far from the former that the `cntr` block, at `Step 3`, starts a new ON-phase at the end of the $\Delta t_{\text{ON}} + \Delta t_{\text{OFF}}^{\min}$ time interval. This does not happen if $R_o^{\text{new}} > R_o^{\text{old}}$ since σ_S^{new} moves below σ_S^{old}. The first situation is sketched in the left panel of Fig. 6, assuming for simplicity that the load variation takes place exactly at the end of the $\Delta t_{\text{ON}} + \Delta t_{\text{OFF}}^{\min}$ time interval when the CCM trajectory is in ϵ_3. Since the `cntr` block locates the trajectory below σ_S^{new}, the periodic steady state is abandoned and transient evolution begins. In this case, it has been assumed that after Δt_{ON} the trajectory is above σ_S^{new} in δ_1. In the right panel of Fig. 6, the σ_S^{new} half-line is moved below σ_S^{old} when the load is changed once more at the end of the $\Delta t_{\text{ON}} + \Delta t_{\text{OFF}}^{\min}$ time interval. In this case, the completion of the OFF phase in δ_2 is feasible.

Analogous considerations can be done if we assume that the load variation takes place at a generic $\tilde{t}$ in the $\Delta t_{\text{ON}} + \Delta t_{\text{OFF}}^{\min}$ time interval. In this case, since R_o is changed, the periodic steady state is abandoned right at $\tilde{t}$ and transient evolution begins. Even in this case, to determine the onset of transient control saturation it is necessary to ensure that at the end of the minimum OFF-phase the trajectory is above σ_S^{new}. It is easy to see that, if the load variation occurs once the minimum OFF-phase is completed, the control is not saturated in the current ON-phase and OFF-phase cycle.

To derive a sufficient condition to detect control saturation in load transients, at first, it is necessary to ensure that control saturation does not occur at steady state. This can be done by following the strategy presented in Section III-A.

By introducing the $(R_o^{\text{old}}, R_o^{\text{new}})$ plane, it is possible to identify the $\mathcal{Q}$ safe region in which both the current and the new value of R_o fulfill the bouncing condition (7) (i.e., $R_o > R_o^{\lim}$), and $R_o > R_o^{\delta\chi}$ with $R_o^{\delta\chi} < R_o^{\text{CrCM}}$.

To determine the onset of control saturation in load transients, it is sufficient to guarantee that the trajectory of the COT converter, at the end of the minimum OFF-phase, lies above σ_S^{new} whatever the $\tilde{t}$ time instant in the $\Delta t_{\text{ON}} + \Delta t_{\text{OFF}}^{\min}$ time interval at which there was the $R_o^{\text{old}} \to R_o^{\text{new}}$ transition. The locus of points on the $(R_o^{\text{old}}, R_o^{\text{new}})$ plane such that $(\imath_L, v_C) \in \sigma_S^{\text{new}}$ once the minimum OFF-phase is completed should be computed for any value of $R_o^{\text{old}} \in \mathcal{Q}$ and for any point of the steady state orbit in the $\Delta t_{\text{ON}} + \Delta t_{\text{OFF}}^{\min}$ time interval. To do that one should compute the $\boldsymbol{\gamma}(R_o^{\text{old}})$ steady state solution of the COT converter for all of such R_o^{old} values. To reduce numerical burden, given R_o^{old} it is possible to focus on the trajectory originated in ζ and find out the limit R_o^{new} value such that $\delta(R_o^{\text{new}}, R_o^{\text{old}}, \tilde{t}) \in \sigma_S^{\text{new}}$ (see Fig. 3). Note that δ depends on the current and next value of R_o and the time instant at which the load is changed. According to the piecewise linear nature of the vector field in (3), the structure of the trajectory is such that it is sufficient to compute the limit value of R_o^{new} for $\tilde{t}$ at the beginning of the ON-phase and at the end of the minimum OFF-phase only. Intermediate values of $\tilde{t}$ correspond to intermediate values of R_o^{new}.

The use of the trajectory originated in ζ instead of $\boldsymbol{\gamma}(R_o^{\text{old}})$ yields a more restrictive but easier to compute constraint on R_o^{new}. For $\tilde{t}$ at the end of the minimum OFF-phase, the limit value of R_o^{new} can be derived analytically. This is not true for $\tilde{t}$ at the beginning of the ON-phase but, in any case, the computation of the orbit from ζ to $\delta(R_o^{\text{new}}, R_o^{\text{old}}, \tilde{t})$ does not require any iterative method or long-lasting transient simulations that in turn are needed to derive $\boldsymbol{\gamma}(R_o^{\text{old}})$.

The strategy discussed above does not work if $R_o^{\text{old}} < R_o^{\delta\chi}$, since in this case, the orbit from ζ arrives by definition in δ after a minimum OFF-phase. In order to avoid the computation of $\boldsymbol{\gamma}(R_o^{\text{old}})$, it is possible to derive an analogous condition considering the trajectory originated from χ as the reference one. For $R_o^{\text{old}} < R_o^{\delta\chi}$, the χ point is the one on σ_S characterized by a minimum OFF-phase. If the choice of R_o^{new} ensures that, given $\tilde{t}$, the trajectory originated in χ belongs to σ_S^{new} this occurs for all the point belonging to σ_S at the right of χ. Obviously this condition is no longer a sufficient condition to detect the onset of control saturation in load transients since the R_o^{old} value does not guarantee it in and of itself. This condition should then be handled with care and basically only if one is able to estimate the intersection of $\boldsymbol{\gamma}(R_o^{\text{old}})$ with σ_S (ϵ_1 in Fig. 6). In fact, assuming that the load transient causes a transient dynamics not "too far" from $\boldsymbol{\gamma}(R_o^{\text{old}})$, the condition is as much safe as much that point is far from χ.

TABLE I
COT CONVERTER CIRCUIT PARAMETER VALUES

Name	Value	Name	Value	Name	Value
C_o	35.3 µF	R_e	12.3 mΩ	R_p	30 mΩ
L	470 nH	E	5 V	v_r	625 mV
R_a	200 Ω	R_b	330 Ω	Δt_{ON}	118 ns
$\Delta t_{\text{OFF}}^{\min}$	177 ns				

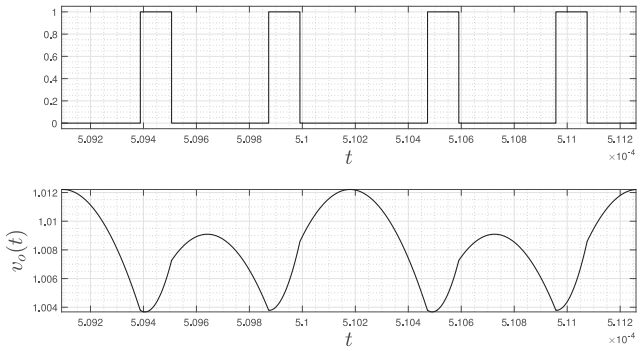

Fig. 7. Upper trace: Comparator output. Lower trace: The $v_o(t)$ output voltage.

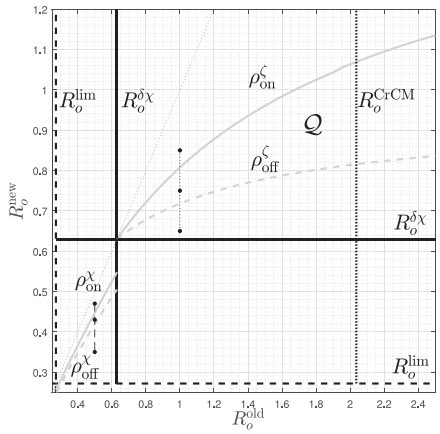

Fig. 8. ρ_{ON}^{ζ} and $\rho_{\text{OFF}}^{\zeta}$ represent the limit value of R_o^{new} as a function of R_o^{old}, that have been obtained with a load variation occurring at the beginning of the ON-phase and at the end of the minimum OFF-phase, respectively.

V. CASE STUDY

A. Numerical Simulations

To focus on a practical example, we consider a well behaving COT converter with the parameter values reported in Table I. To force the onset of subharmonics, we modify the values to $C_o = {}^{35.3\,\mu\text{F}}/_{3}$, $R_e = {}^{12.3\,\text{m}\Omega}/_{3}$ obtaining $2C_oR_e \approx 96.49$ ns and $R_o^{\lim} \approx 2.463\,\Omega$. We determine the steady-state solution of the COT with $R_o = 1.8\,\Omega < R_o^{\lim}$. The results are shown in Fig. 7, subharmonics are clearly visible.

We now consider the original value of COT parameters and check the onset of a minimum off cycle. For this configuration we have $R_o^{\lim} \approx 0.272\,\Omega$, $R_o^{\delta\chi} \approx 0.630\,\Omega$, $R_o^{\text{CrCM}} \approx 2.04\,\Omega$, and $2C_oR_e = 868.38\,\text{ns} > \Delta t_{\text{on}}$. The $\mathcal{Q}$ region in Fig. 8 is bounded by the constraints $R_o^{\text{old}} > R_o^{\delta\chi}$ and $R_o^{\text{new}} > R_o^{\delta\chi}$.

The ρ_{ON}^{ζ} and $\rho_{\text{OFF}}^{\zeta}$ curves in Fig. 8 represent the limit value of R_o^{new} as a function of R_o^{old}, that have been obtained with a load variation occurring at the beginning of the ON-phase and at the end of the minimum OFF-phase, respectively. As an example, we consider three variations from $R_o^{\text{old}} = 1\,\Omega$ to R_o^{new} equal to 0.85 , 0.75 , and 0.65 Ω. In the first case (see Fig. 9, left panel) the points δ and π_ζ are above σ_S^{new}, being the former the last point of the trajectory originated in ζ and computed assuming $R_o \equiv R_o^{\text{old}}$ (viz. the load is varied in δ at the end of the minimum OFF-phase) and the latter the trajectory originated in ζ and computed assuming $R_o \equiv R_o^{\text{new}}$ (viz. the load is varied in ζ at the beginning of the ON-phase). If the $\boldsymbol{\gamma}(R_o^{\text{old}})$ limit cycle is considered, also $\delta_\nu \in \sigma_{\text{OFF}}^{\min}$ and π_ν, i.e., the last point of the trajectory originated in ν and computed assuming $R_o \equiv R_o^{\text{new}}$, are above σ_S^{new} too.

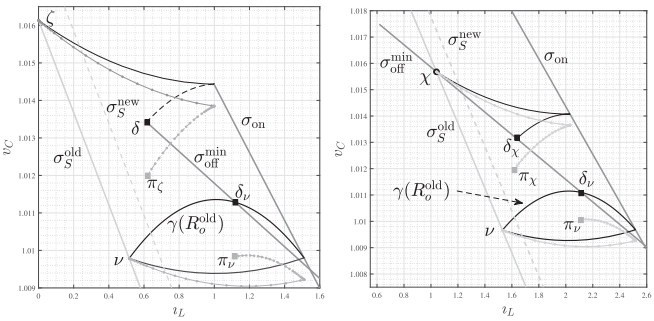

Fig. 9. Left panel: $R_o^{\text{old}} = 1\,\Omega$ and $R_o^{\text{new}} = 0.85\,\Omega$. Right panel: $R_o^{\text{old}} = 0.5\,\Omega$ and $R_o^{\text{new}} = 0.47\,\Omega$.

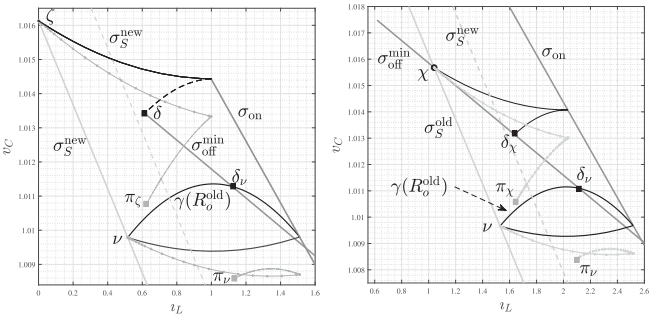

Fig. 10. Left panel: $R_o^{\text{old}} = 1\,\Omega$ and $R_o^{\text{new}} = 0.75\,\Omega$. Right panel: $R_o^{\text{old}} = 0.5\,\Omega$ and $R_o^{\text{new}} = 0.43\,\Omega$.

This is not true for $R_o^{\text{new}} = 0.75\,\Omega$ as it can be seen in Fig. 10 (left panel). In this case, δ and π_ζ are respectively above and below σ_S^{new}. This means that the $1 \to 0.75\,\Omega$ load variation, according to the sufficient condition that we derived, will cause control saturation if it is applied at the beginning of the ON-phase. This is coherent with the position of the $(1, 0.75)$ point on the $(R_o^{\text{old}}, R_o^{\text{new}})$ plane (see Fig. 8): It lies in between ρ_{ON}^{ζ} and $\rho_{\text{OFF}}^{\zeta}$. Actually, since δ_ν and π_ν in Fig. 10 lie above σ_S^{new}, as anticipated in Section IV, the sufficient condition that we are considering is restrictive. Nevertheless it provides a significant design condition since it can be applied without deriving ν, viz. the $\boldsymbol{\gamma}(R_o^{\text{old}})$ limit cycle.

If $R_o^{\text{new}} = 0.65\,\Omega$, (see Fig. 11, left panel) both δ and π_ζ are below σ_S^{new} and consequently, the $1 \to 0.65\,\Omega$ load variation is certainly causing control saturation. By considering δ_ν and π_ν it can be realized that actually control saturation will not happen if the load variation is applied at the end of the minimum OFF-phase, but it will occur if load variation is applied at the beginning of the ON-phase.

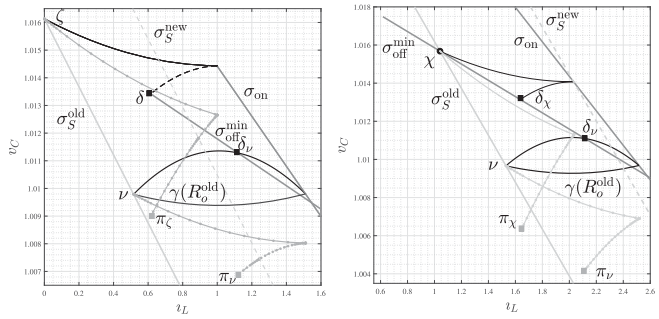

Fig. 11. Left panel: $R_o^{\text{old}} = 1\,\Omega$ and $R_o^{\text{new}} = 0.65\,\Omega$. Right panel: $R_o^{\text{old}} = 0.50\,\Omega$ and $R_o^{\text{new}} = 0.35\,\Omega$.

Let us now consider $R_o^{\text{off}} = 0.5\,\Omega$, i.e., an initial load value not belonging to the $\mathcal{Q}$ safe region. As it can be noticed from Fig. 9 (right panel), the δ point lies below $\sigma_{\text{OFF}}^{\min}$ and consequently ζ can not be used to estimate the effect of load variations. For this purpose, the χ and the associated δ_χ and π_χ points are considered, being the former and the latter the last point of the trajectory originated in χ with R_o equal to R_o^{old} and R_o^{new}, respectively. As an example, in Fig. 9 (right panel), the $0.5 \rightarrow 0.47\,\Omega$ transition is considered. Both δ_χ and π_χ are above σ_S^{new} and this is coherent with the position of the $(0.5, 0.47)$ point above ρ_{ON}^{χ} and ρ_{OFF}^{χ} (see Fig. 8). Hence this load transition does not imply the saturation of the controller provided that in transient the orbit of the COT converter does not visit σ_S in between ζ and χ. In Fig. 10 (right panel), $R_o^{\text{new}} = 0.43\,\Omega$ and the π_χ point is below σ_S^{new}. This does not occur for π_ν. For $R_o^{\text{new}} = 0.35\,\Omega$ (see Fig. 11, right panel), δ_χ, π_χ, δ_ν, and π_ν are all below σ_S^{new} and the controller is saturated.

For both $R_o^{\text{old}} = 1.0\,\Omega$ and $R_o^{\text{old}} = 0.5\,\Omega$ we derived in simulation the limit load transition (applied at the beginning of the ON-phase) implying the saturation of the controller (i.e., $\pi_\nu \in \sigma_S^{\text{new}}$) and we obtained $R_o^{\text{new}} = 0.71\,\Omega$ and $R_o^{\text{new}} = 0.41\,\Omega$, respectively. With respect to these values, the (conservative) estimates derived by our approach is almost 10% larger.

To investigate how the derived conditions vary as a function of the circuit parameters, R_o^{lim}, $R_o^{\delta\chi}$, and R_o^{CrCM} have been derived by varying C_o in the $[20\,\mu\text{F}, 60\,\mu\text{F}]$ interval and $L \in [450\,\text{nH}, 1500\,\text{nH}]$. The results are reported in Fig. 12. The variations of R_o^{lim}, $R_o^{\delta\chi}$, and R_o^{CrCM} when C_o is fixed at 35.3 μF as in Table I, and L is varied in the aforementioned interval can be observed following the white dashed lines in Fig. 12.

The ρ_{ON}^{ζ} and $\rho_{\text{OFF}}^{\zeta}$ curves (parametrized by L) have been derived. The results are reported in Fig. 13 for four suitable values of L listed in the figure caption. It can be noticed that, as L increases, the distance between ρ_{ON}^{ζ} and $\rho_{\text{OFF}}^{\zeta}$ increases too. This implies that applying an $R_o^{\text{old}} \rightarrow R_o^{\text{new}}$ transition at the beginning of the ON-phase becomes more critical w.r.t. doing it at the end of the minimum OFF-phase if one wants to avoid control saturation. On the contrary, if one wants to exploits the maximum performance of COT converter in terms of speed, to apply the load variation at the beginning of the ON-phase becomes more and more convenient. Analogous results can be obtained as far as the ρ_{ON}^{χ} and ρ_{OFF}^{χ} curves are concerned.

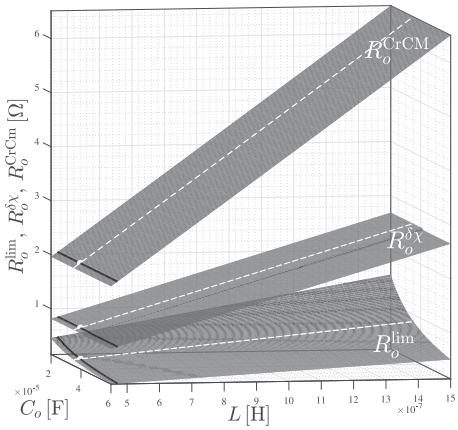

Fig. 12. R_o^{lim}, $R_o^{\delta\chi}$, and R_o^{CrCM} as a function of C_o and L. White dots (at the intersection between black solid and white dashed lines) have been computed for C_o and L as in Table I.

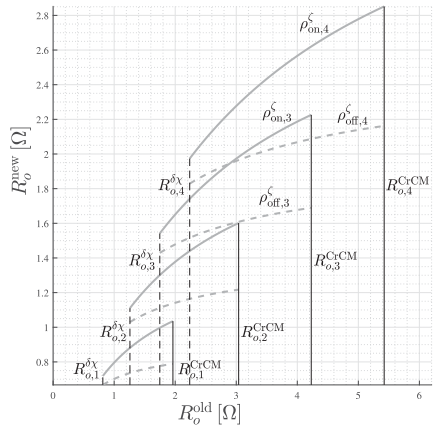

Fig. 13. ρ_{ON}^{ζ} (solid gray) and $\rho_{\text{OFF}}^{\zeta}$ (dashed gray) curves parametrized by L. $\rho_{\text{ON},j}^{\zeta}$ and $\rho_{\text{OFF},j}^{\zeta}$ have been computed for $R_o^{\text{old}} \in [R_{o,j}^{\delta\chi}, R_{o,j}^{\text{CrCM}}]$ ($j = 1, \ldots, 4$). The inductance value for $j = 1, \ldots, 4$ is 450, 700, 975, and 1250 nH, respectively.

B. Experimental Results

The experimental results in this section have as target to show that the $\Delta t_{\text{OFF}}^{\min}$ prediction when there is a step increase of load is reliable and adequately accurate.

As benchmark we used the evaluation board of the MIC4950 COT converter by MICROCHIP TECHNOLOGY INC. The parameters of the COT converter are still those in Table I. The values and derating of parameters of some elements, such as the ESR and C_o capacitance were measured with the AGILENT E4980A impedance meter. The load is varied by connecting a resistor (that we refer to as R_x) in parallel to R_o. One terminal of R_x is connected to R_o and the other terminal to the drain of a MOSFET (M_x), whose source is connected to ground. The gate is driven by a 6 V square waveform at 1 kHz. The MOSFET turn-ON connects R_x in parallel to R_o.

By referring to the $\mathcal{Q}$ region of Fig. 8, we performed a step variation of R_o from 1.01 to 0.857 Ω (both measured). Our approach predicts that there is not any cycle at $\Delta t_{\text{OFF}}^{\min}$. The experimental results are shown in Fig. 14.

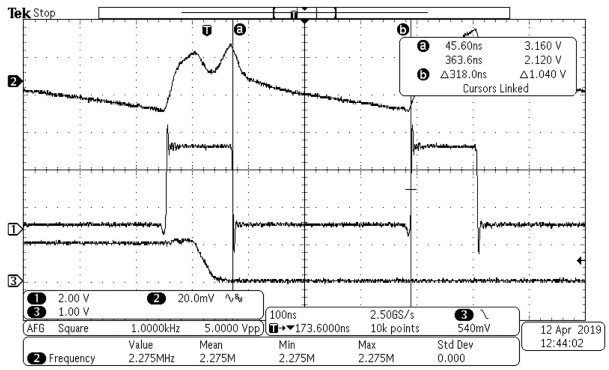

Fig. 14. Experimental waveform related to the 1.01 to 0.857 Ω step variation of the R_o. The set up of the measure is in the figure itself. Trace 1: Driving signal of the COT converter. Trace 2: Output voltage (AC coupling). Trace 3: Drain voltage of the M_x MOSFET.

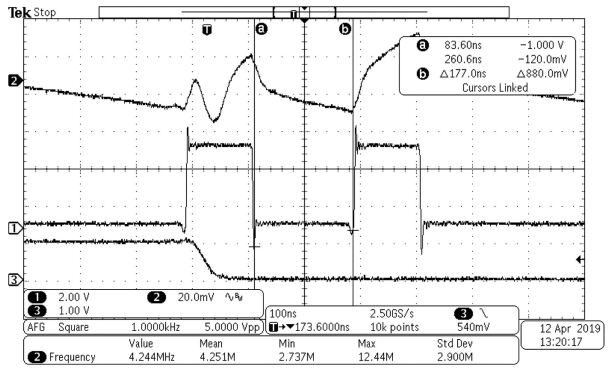

Fig. 15. Experimental waveform related to the 1.01 to 0.690 Ω step variation of R_o. Traces have the same meaning as those in Fig. 14.

All waveforms are recorded with the TEKTRONIX MDO3024 oscilloscope. The trace 3 shows the drain voltage of the M_x MOSFET. We see that it drops in 40 ns, i.e., sufficiently faster than Δt_{on}. It is thus reasonable to assume that the load undergoes a step variation. The step (falling front of trace 3) is applied inside the Δt_{on} time interval which corresponds to the upper limiting curve in Fig. 8. The full application of the step ends before the beginning of the $\Delta t_{\text{OFF}}^{\min}$ cycle. The first Δt_{OFF} cycle after the application of the step variation lasts 318 ns $> \Delta t_{\text{OFF}}^{\min}$ as predicted by our approach.

We then varied R_o from 1.01 to 0.690 Ω that we predict will cause at least one cycle at $\Delta t_{\text{OFF}}^{\min}$. The new load value is below the dashed curve in Fig. 8. Note that we choose R_o values that are very close to the upper and lower curves in Fig. 8 to show the accuracy of the proposed approach.

The experimental results are shown in Fig. 15.

The application of the step variation ends once more inside Δt_{on}. We clearly see that the first cycle of the COT converter after the step variation of the load lasts exactly $\Delta t_{\text{OFF}}^{\min} = 177$ ns as predicted.

We did other experiments with different sets of parameters of the COT converter; results always confirmed predictions.

VI. Conclusion

We have considered a commercial COT converter, i.e., the MIC4950 by MICROCHIP TECHNOLOGY INC., and after suitable but reasonable simplifications we have applied fundamentals of nonlinear dynamics to derive boundary expressions to check the onset of subharmonic oscillations and the saturation of the COT converter controller. We derived the value of the R_o output resistance below which the unwanted onset of subharmonics during the steady state working of the COT converter is observed. The limit value (7) is derived as a function of the other values of the design parameters such as, for example, the inductance value, the output capacitance value, and the input voltage. We also derived conditions that show if after a step variations of the load there is at least one subsequent working cycle of the COT converter at minimum off-time, i.e., with the controller saturated. As far as we know, this is a novel result extremely useful to designer never before presented in the literature. The proposed approach was tested versus experimental results, that always confirmed predictions.

Appendix A
Nomenclature Description List

$\Delta t_{\text{OFF}}^{\min}$	Minimum duration of the OFF-phase.
Δt_{OFF}	Overall duration of the OFF-phase.
Δt_{ON}	Duration of the ON-phase.
ρ_S	Manifold induced by the COT converter control block, reached by trajectories at the end of the OFF-phase.
η	Normal vector to ρ_S.
ρ_D	Manifold induced by the D low-side switch.
$\imath_\zeta$	Lower limit of $\imath_L$ ruled by the reverse current limit implemented for the low-side synchronous rectifier switch.
ζ	$\zeta = \rho_S \cap \rho_D$ is the origin of the σ_S, σ_D half-lines.
σ_{ON}	Locus of points reached in Δt_{ON} (at the end of the ON-phase) by orbits originated on σ_{S}.
$\sigma_{\text{OFF}}^{\min}$	Locus of points reached in $\Delta t_{\text{OFF}}^{\min}$ (end of the minimum OFF-phase) by orbits originated on σ_{ON}.
δ	Origin of the $\sigma_{\text{OFF}}^{\min}$ half-line reached in $\Delta t_{\text{ON}} + \Delta t_{\text{OFF}}^{\min}$ by a trajectory originated in ζ.
$\mathcal{R}_m$	Locus of points lying both at the right of the ρ_D line and below the ρ_S line.
$\mathcal{R}_M$	Locus of points lying both at the right of the ρ_D line and above the ρ_S line.
$\Gamma_{\text{ON}}^{(k)} - \Gamma_{\text{OFF}}^{(k)}$	$k-$th segment of a generic orbit of the COT accounting for the $k-$th ON-phase ($\Gamma_{\text{ON}}^{(k)}$) and the $k-$th OFF-phase ($\Gamma_{\text{OFF}}^{(k)}$).
χ	$\chi = \sigma_{\text{OFF}}^{\min} \cap \sigma_S$ exists iff the trajectory from ζ reaches σ_S in $\Delta t_{\text{OFF}}^{\min}$.
$\mathcal{C}_I$	Two-segment steady-state solution whose $\Gamma_{\text{ON}}^{(1)} - \Gamma_{\text{OFF}}^{(1)}$ segment originates on σ_S and ends in $\mathcal{R}_m$.
$\mathcal{C}_{II}$	Two-segment steady-state solution whose $\Gamma_{\text{ON}}^{(1)} - \Gamma_{\text{OFF}}^{(1)}$ segment originates and ends in two different points of σ_S.

R_o^{CrCM} Limit value of R_o fixing the boundary between CCM and DCM.

R_o^{lim} Sufficient limit value of R_o to avoid pulse bursting.

$R_o^{\delta\chi}$ Limit value of R_o such that $\chi \equiv \delta \in \sigma_S$.

R_o^{old}, R_o^{new} R_o values before and after the load transition.

$\boldsymbol{\gamma}(R_o)$ Single-segment steady state orbit for a given R_o.

ν $\nu = \boldsymbol{\gamma} \cap \sigma_{\text{ON}}$ is the starting point of the ON-phase and the ending point of the OFF-phase of $\boldsymbol{\gamma}(R_o)$.

π_ζ, π_ν, π_χ Points reached in $\Delta t_{\text{ON}} + \Delta t_{\text{OFF}}^{\text{min}}$ by a trajectory originated in ζ, ν, χ with $R_o \equiv R_o^{\text{new}}$.

δ_ν, δ_χ Points reached in $\Delta t_{\text{ON}} + \Delta t_{\text{OFF}}^{\text{min}}$ by a trajectory originated in ν, χ with $R_o \equiv R_o^{\text{old}}$.

ρ_{ON}^{ζ}, $\rho_{\text{OFF}}^{\zeta}$ For a given value $R_o^{\text{lim}} < R_o^{\text{CrCM}} < R_o^{\text{old}}$ of the output resistance, $R_o^{\text{new}} = \rho_{\text{ON,OFF}}^{\zeta}(R_o^{\text{old}})$ is the sufficient limit value of load variation occurring either at the beginning of the ON-phase or at the end of the minimum OFF-phase implying transient control saturation.

ρ_{ON}^{χ}, ρ_{OFF}^{χ} For a given value $R_o^{\text{lim}} < R_o^{\text{old}} R_o^{\text{CrCM}}$ of the output resistance, $R_o^{\text{new}} = \rho_{\text{ON,OFF}}^{\zeta}(R_o^{\text{old}})$ is the estimated limit value of load variation occurring either at the beginning of the ON-phase or at the end of the minimum OFF-phase implying transient control saturation.

APPENDIX B
ON THE PULSE-BURSTING CONDITION

The very simple $2C_oR_e > \Delta t_{\text{ON}}$ condition used to ensure that the COT converter does not suffer of the pulse-bursting drawback can be derived from the more detailed (6) condition.

By setting $R_a = 0$ and $R_b \to +\infty$, the v_m voltage in Fig. 1 equals v_o, i.e., the voltage partitioner is completely removed. Setting in (6) $\imath_\zeta = 0$, $v_r = v_o$ and defining $\tau = C_oR_e$, we obtain $R_o > \frac{L_o v_o}{\tau(E - v_o)}$. We compute the $\Delta\imath_L$ current during the Δt_{ON} time interval by assuming that the v_o voltage remains constant $L_0 \Delta\imath_L / \Delta t_{\text{ON}} = E - v_o$, from which we have $L_0/(E-v_o) = \Delta t_{\text{ON}}/\Delta\imath_L$. In the CCM condition the $\imath_o = v_o/R_o$ output current can be assumed equal to the average value of $\imath_L$, which is a positive constant (it is null in CRCM), plus $\Delta\imath_L/2$. We can now write $v_o/R_o \geq \Delta\imath_L/2$, where the equality applies in CRCM. At the end we obtain

$$C_oR_e \equiv \tau \geq \frac{L_o}{E - v_o}\frac{v_o}{R_o} \geq \frac{\Delta t_{\text{ON}}}{\Delta\imath_L}\frac{\Delta\imath_L}{2} = \frac{\Delta t_{\text{ON}}}{2}. \quad (8)$$

In DCM, the (8) condition is incorrect; since $v_o/R_o < \Delta\imath_L/2$ while the (6) condition is still valid even when useless; since in general R_o is very large and greater than R_o^{lim}.

REFERENCES

[1] K. Hariharan, S. Kapat, and S. Mukhopadhyay, "Constant on/off-time hybrid modulation in digital current-mode control using event-based sampling," *IEEE Trans. Power Electron.*, vol. 34, no. 4, pp. 3789–3803, Apr. 2019.

[2] W. Fu, S. T. Tan, M. Radhakrishnan, R. Byrd, and A. A. Fayed, "A DCM-only buck regulator with hysteretic-assisted adaptive minimum-on-time control for low-power microcontrollers," *IEEE Trans. Power Electron.*, vol. 31, no. 1, pp. 418–429, Jan. 2016.

[3] C. Ni and T. Tetsuo, "Adaptive constant on-time (D-CAP™) control study in notebook applications," Texas Instruments, Dallas, TX, USA, Tech. Rep., 2007. [Online]. Available: http://www.ti.com/lit/an/slva281b/slva281b.pdf

[4] J. Sun, "Characterization and performance comparison of ripple-based control for voltage regulator modules," *IEEE Trans. Power Electron.*, vol. 21, no. 2, pp. 346–353, Mar. 2006.

[5] J. Sun, "Small-signal modeling of variable-frequency pulsewidth modulators," *IEEE Trans. Aerosp. Electron. Syst.*, vol. 38, no. 3, pp. 1104–1108, Jul. 2002.

[6] J. Li and F. C. Lee, "Modeling of v^2 current-mode control," *IEEE Trans. Circuits Syst. I: Reg. Papers*, vol. 57, no. 9, pp. 2552–2563, Sep. 2010.

[7] W. Yang *et al.*, "A constant-on-time control dc–dc buck converter with the pseudowave tracking technique for regulation accuracy and load transient enhancement," *IEEE Trans. Power Electron.*, vol. 33, no. 7, pp. 6187–6198, Jul. 2018.

[8] J. Wang, J. Xu, and B. Bao, "Analysis of pulse bursting phenomenon in constant-on-time-controlled buck converter," *IEEE Trans. Ind. Electron.*, vol. 58, no. 12, pp. 5406–5410, Dec. 2011.

[9] J. Wang, B. Bao, J. Xu, G. Zhou, and W. Hu, "Dynamical effects of equivalent series resistance of output capacitor in constant on-time controlled buck converter," *IEEE Trans. Ind. Electron.*, vol. 60, no. 5, pp. 1759–1768, May 2013.

[10] T. Qian, "Subharmonic analysis for buck converters with constant on-time control and ramp compensation," *IEEE Trans. Ind. Electron.*, vol. 60, no. 5, pp. 1780–1786, May 2013.

[11] R. Redl and J. Sun, "Ripple-based control of switching regulators—An overview," *IEEE Trans. Power Electron.*, vol. 24, no. 12, pp. 2669–2680, Dec. 2009.

[12] J. L. Na Kong, D. S. Ha, and F. C. Lee, "Off-time prediction in digital constant on-time modulation for dc-dc converters," in *Proc. IEEE Int. Symp. Circuits Syst.*, 2008, pp. 3270–3273.

[13] P. Nora and V. Uzum, "Application guidelines for the microchip constant on-time regulators with internal ripple injection," , Microchip Technology Inc., Chandler, AZ, USA, Tech. Rep., 2017. [Online]. Available: http://ww1.microchip.com/downloads/en/AppNotes/00002526A.pdf

[14] D. Mohol, G. Bhagwat, and A. Garg, "Transient response versus ripple—An analysis of ripple injection techniques used in hysteretic controllers," Texas Instruments, Dallas, TX, USA, Tech. Rep., 2014. [Online]. Available: http://www.ti.com/lit/an/slva653/slva653.pdf

[15] *MIC4950 Hyper Speed Control 5A Buck Regulator.* rev. 1.1, (2014), Microchip Technology Inc. [Online]. Available: http://ww1.microchip.com/downloads/en/DeviceDoc/MIC4950.pdf

[16] "AN-1481 controlling output ripple and achieving ESR independence in constant on-time (COT) regulator designs," Texas Instruments, Dallas, TX, USA, Tech. Rep., 2013. [Online]. Available: http://www.ti.com/lit/an/snva166a/snva166a.pdf

[17] I. Novak and J. R. Miller, *Frequency-Domain Characterization of Power Distribution Networks*, 1st ed. Norwood, MA, USA: Artech House, 2007.

[18] E. Bogatin, I. Novak, S. Sandler, L. Smith, and B. Brim, "Target impedance and rogue waves," presented at the 2016 Panel discussion in DesignCon2016, Santa Clara, CA, USA, Jan. 2016.

[19] I. Novak, *Power Distribution Network Design Methodologies*. Chicago, IL, USA: Int. Eng. Consortium, 2008.

[20] W. Chen *et al.*, "Reduction of equivalent series inductor effect in delay-ripple reshaped constant on-time control for buck converter with multilayer ceramic capacitors," *IEEE Trans. Power Electron.*, vol. 28, no. 5, pp. 2366–2376, May 2013.

[21] S. Sandler and H. Barnes, "Introduction to power integrity," presented at the 2016 20th IEEE Workshop on Signal and Power Integrity, Turin, Italy, May 2016.

[22] A. P. Chandrakasan, S. Sheng, and R. W. Brodersen, "Low-power CMOS digital design," *IEEE J. Solid-State Circuits*, vol. 27, no. 4, pp. 473–484, Apr. 1992.

[23] M. Di Bernardo, C. Budd, A. Champneys, and P. Kowalczyk, *Piecewise-Smooth Dynamical Systems, Theory and Applications*. Berlin, Germany: Springer-Verlag, 2008.

Federico Bizzarri (M'12–SM'14) was born in Genoa, Italy, in 1974. He received the Laurea (M.Sc.) five-year degree (*summa cum laude*) in electronic engineering and the Ph.D. degree in electrical engineering from the University of Genoa, Genoa, Italy, in 1998 and 2001, respectively.

Since October 2018, he has been an Associate Professor with the Electronic and Information Department of the Politecnico di Milano, Milan, Italy. He is a Research Fellow of the Advanced Research Center on Electronic Systems for Information and Communication Technologies "E. De Castro" (ARCES), University of Bologna, Bologna, Italy.

Dr. Bizzarri served as an Associate Editor of the IEEE TRANSACTIONS ON CIRCUITS AND SYSTEMS — PART I from 2012 to 2015 and was awarded as one of the 2012–2013 Best Associate Editors of this journal.

Paolo Nora received the Dr. Ing. degree in electronics engineering *summa cum laude* from the University of Pavia, Pavia, Italy, in 1992.

Currently he is a Senior Staff Strategic Applications Engineer at Microchip Technology, Analog Power and Interface Division, Chandler, AZ, USA. He previously covered IC Design and Applications Engineering positions in the field of Power Management at various semiconductor companies (ST Microelectronics, Maxim Integrated, National Semiconductor, Texas Instruments, and Micrel). In 1996–1997, he was a Visiting Engineer for ST Microelectronics at the Virginia Power Electronics Center (VPEC) Blacksburg, VA, USA, where he worked on single-phase PFC architectures and VRM design. His current research interests include architectural definition and optimization of analog point-of-load dc–dc converters and power integrity.

Angelo Brambilla (M'16) received the Dr. Ing. degree in electronics engineering from the University of Pavia, Pavia, Italy, in 1986.

Currently he is a Full Professor at the Dipartimento di Elettronica e Informazione, Politecnico di Milano, Milano, Italy, where he has been working in the areas of circuit analysis and simulation.